Trap-controlled Field Instabilities in Photoconducting CdS Caused by Field-quenching*

Abstract: The formation of stationary high-field domains adjacent to cathode or anode, dependent on the contact potential of the electrodes, their widening with increased applied voltage and their transition into two types of moving domains are discussed. Domains which move under deformation of the domain profile and usually dissolve before they reach the anode, and nearly undeformed moving domains are described. The structure and kinetics of these domains are directly observed using the Franz-Keldysh effect and photographs of typical domain forms are presented.

Introduction

The negative differential conductivity in CdS:Cu,Alplatelets for photocurrent densities below 10⁻² A/cm² is due to a decrease of the electron density n by several orders of magnitude with field E between 30 and 100 kV/cm, caused by field-quenching^{1,2} of the photoconductivity (a certain type of field-enhanced recombination due to redistribution of holes from slow to fast recombination centers³). Compared to n(E) only negligible changes of the mobility μ occur in this field range. Highfield domains occur in the range of N-shaped negative differential conductivity⁴ and can be made directly visible^{1,5} using the Franz-Keldysh effect: They appear as darker areas in photographs of the crystal taken in monochromatic light at the band edge. Depending on boundary conditions, they are either stationary adjacent to one electrode or move rather slowly through the crystal, with typical velocities of 10^{-3} to 10^{-1} cm/sec, indicating trap controlled major space charge regions.

General discussion of stationary domains (Type I)

It has been shown⁷⁻⁹ that the time-independent Poisson and transport equations (for simplicity given for only one relevant coordinate)

$$\frac{dE}{dx} = \frac{e}{\epsilon \epsilon_0} \rho(x)$$
and
$$\frac{dn}{dx} = \frac{e}{kT} \left(nE - \frac{j}{e\mu} \right)$$
(1)

contain stationary solutions of domain character. Since the space charge $\rho(x)$ for the trap-controlled case depends on the reaction kinetic model and usually contains numerous sparely known parameters, a qualitative graphic discussion of system (1) is generally used and referred to as field-of-direction-analysis^{1,8,10}. Without going into detail, for which we refer to the original paper, we will discuss here only the essential results of this analysis.

These results are certainly of more general interest since the discussion does not depend on the specific reaction kinetic model and contains only the fact that the carrier density drops in a certain field range steeper than linearly with increasing field, while the mobility remains essentially field-independent. (It shall be mentioned that a similar analysis can be carried out for the Gunneffect as exemplified in Refs. 8, 11 and 12). In Fig. 1 this drop of carrier density with field is shown† by $n_1(E)$, graphs (a). At higher fields $n_1(E)$ increases due to field excitation of carriers, as experimentally observed. 13 The curves $n_2(E)$ in the graphs (a) of Fig. 1 are the drift current curves: $n_2(E) = j/e\mu E$. Close to this curve a physical meaningful solution must lie (heavy arrows in graphs (a), drawn for increasing applied voltages with increasing index). Graphs (b) in the same figure show the corresponding field distributions between cathode (c) and anode (a). Graphs (c) show the current-voltage characteristic with points referring to the type of solution with same index in the upper graphs.

As an example let us discuss the middle column of Fig. 1 in more detail. Experimental results^{13,14} have

^{*} Supported by the Office of Naval Research, Washington, D. C. The author is in the Physics Department, University of Delaware, Newark, Delaware 19711.

 $[\]dagger$ The index 1 at the carrier density indicates that n is calculated for a space-charge-free region of the crystal.

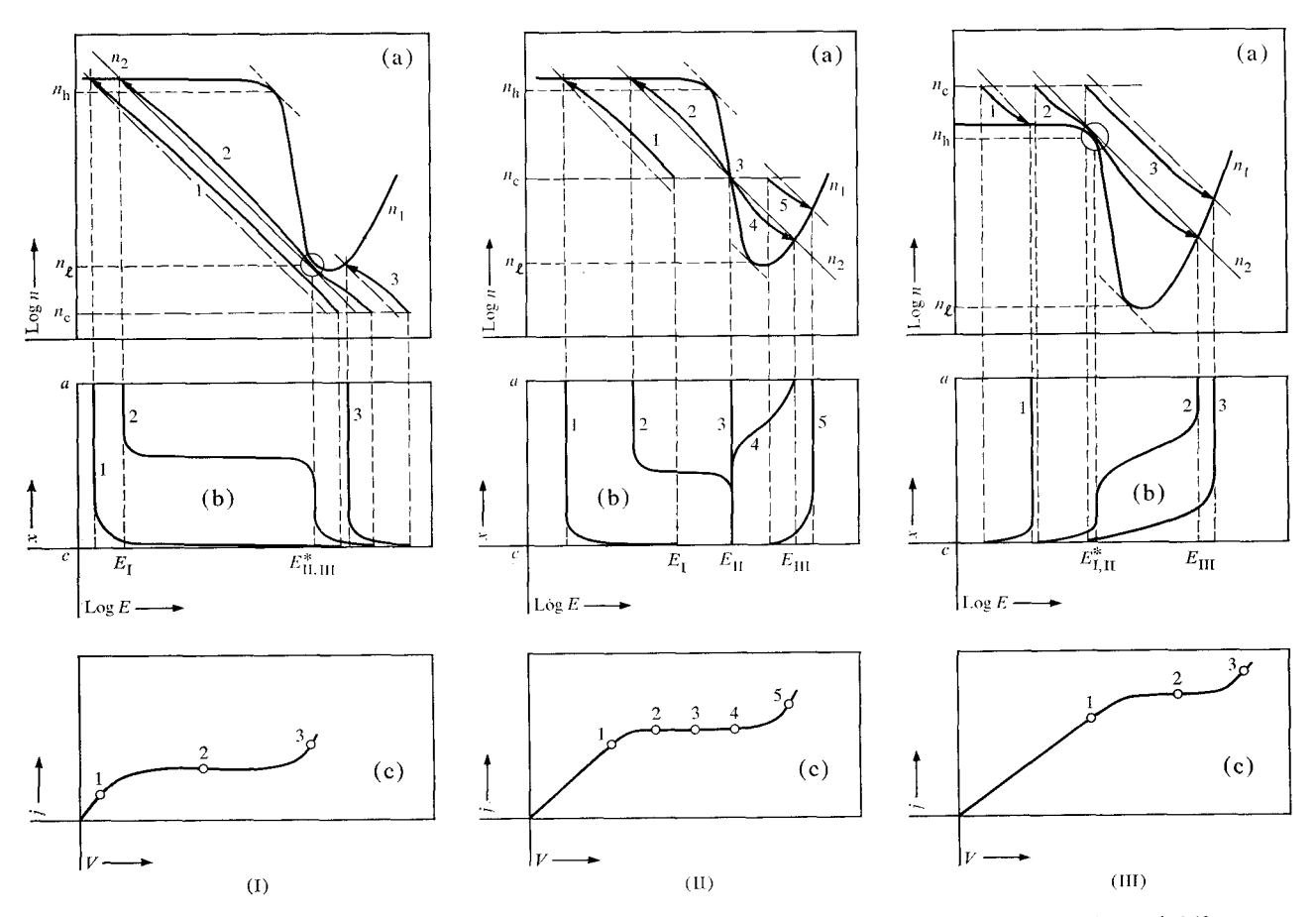


Figure 1 Electron density as a function of electric field (n vs E) in diagrams (a) with quasi neutrality curve $n_1(E)$ and drift current curves $n_2(E)$ for three different currents and projection of the solution curves (1, 2, and 3) for these currents. (b) Field distribution from anode, a, to cathode, c. (c) Current-voltage characteristics for three different boundary conditions. (I) $n_c < n_l$, (II) $n_l < n_c < n_h$, and (III) $n_c > n_l(E = 0)$.

shown that the electron density at the cathode, n_c (n-type CdS), is a physically determining boundary condition. We therefore neglect the behavior at the anode. Assuming for simplicity that n_c is independent of field and current density (for the actual behavior see Ref. 15), at low applied voltage (1) the cathode acts as a Schottky barrier. With increasing voltage a cathode-adjacent high-field domain and current saturation is predicted (2). The domain width should increase with further increasing voltage until it fills the entire space between the electrodes [homogeneous solution, (3)]. Here the entire crystal should be at constant field in the negative differential conductivity range. With still increasing applied voltage a higherfield domain is expected to enter from the anode (4) until it fills about the entire crystal and then current saturation should terminate and the contact should behave as an injecting contact (5).

These predictions are in excellent agreement with the experimental results given in Fig. 2, which show the increasing width of the cathode-adjacent high-field domain

(dark range near cathode at left side) with increasing voltage from 500 to 1750 V. Slightly above 1750 V the entire crystal is homogeneously darkened indicating a homogeneous field. At higher voltage a higher-field domain (darker range) becomes visible adjacent to the anode and at 3200 V fills about a third of the crystal. No field or current oscillations are observed as long as the crystal is narrow enough and "properly" doped (see below).

From the measured domain widths as function of the applied voltage the field strength in both domains can be easily determined as long as the domain width is a linear function of the voltage (neglecting the space-charge region at the end of the domain is justified). In most cases this is experimentally observed. From the saturation current one can immediately obtain the carrier density in the regions of flat-field profile, i.e. the values $n_1(E_I)$, $n_1(E_{II})$ as shown in Fig. 1, II.

If the electron density at the cathode is smaller than n_1 (as defined in Fig. 1) the left column of Fig. 1 applies,

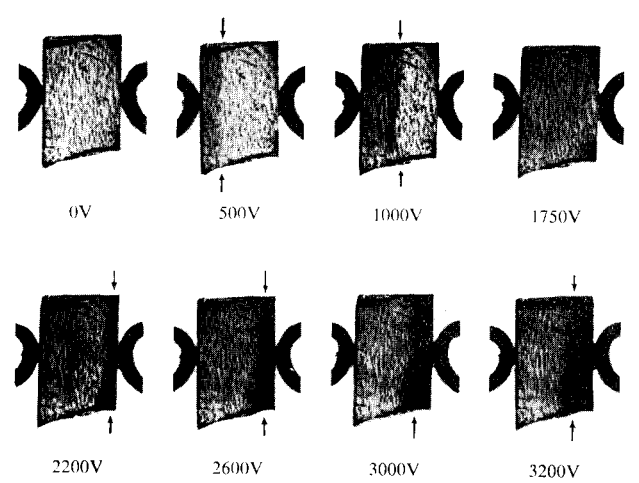


Figure 2 Photographs of CdS platelets taken in band-edge light showing the high-field domains as dark areas adjacent to one electrode.

if $n_c > n_1$ (E = 0), the right column of Fig. 1 applies. The latter case usually is referred to as injecting contact and it is clear that only anode-adjacent high field domains can occur in this case, when the solution squeezes between $n_1(E)$ and $n_2(E)$ [indicated by the circle in graph (a)] and reaches E_{III} .

This again is in agreement with the experiment, as shown in Fig. 3. The left and center columns show the domain behavior similar to Fig. 2 when a crystal with asymmetric electrodes (gold-blocking and indium-injecting) is poled in the reverse direction. In the forward direction (injecting cathode), however, no cathode-adjacent high-field domain is observed preceding the anode-adjacent higher field domain, as shown in the right column of Fig. 3.

These results clearly show that the cathode boundary determines the domain behavior, and, inversely, it indicates that from the domain analysis, the density n_c and herewith the barrier height Ψ_{ms} between metal and semiconductor may be obtained:

$$n_c = N_c \exp -\left(\frac{\Psi_{ms}}{kT}\right), \tag{1}$$

with N_c , the effective level density at the lower edge of the conduction band of the semiconductor. This is, under certain circumstances as described in Ref. 15, indeed the case, and presents a possibility to determine Ψ_{ms} for finite current densities (all other methods determine Ψ_{ms} in the limit of zero current densities).

If one could change n_c for the same crystal (same doping) one could measure different triplets of $n_1(E_i)$ with the described method and therefore determine essentially the entire $n_1(E)$ curve. This is possible with the aid of

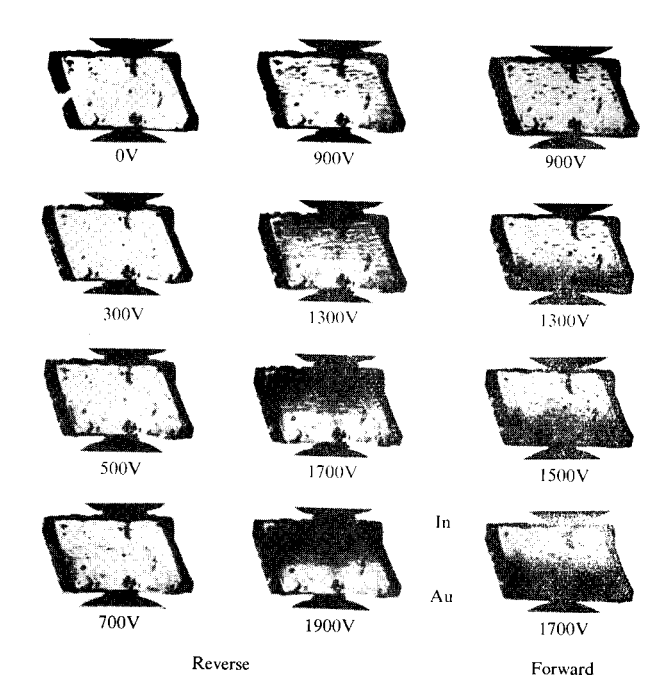
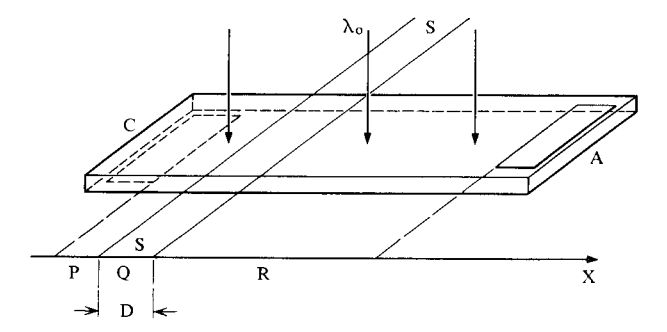


Figure 3 Photographs similar to those in Figure 2, using asymmetric electrodes: upper, indium; lower, gold.

Figure 4 Schematic diagram showing the technique for illuminating the crystal in band-edge light (λ_0) using a shadow (S-S) as a quasi-cathode.



a shadow S-S of different darkness projected across a wider crystal (Fig. 4). If the carrier density in the shadow region Q is smaller than at the cathode (here preferably an injecting cathode) then Q acts as pseudo-cathode and a domain occurs in region R, as shown in Fig. 5. These domains can be analyzed essentially ¹⁶ as discussed above and yield unambiguously the electron density in a space-charge free crystal region as a function of field, provided the mobility is known as a function of the field.

Stationary high-field domains can be made wide enough to accommodate Hall electrodes and to measure¹⁷ the Hall-effect within these domains. This has been done for a number of crystals with different electrodes, yielding

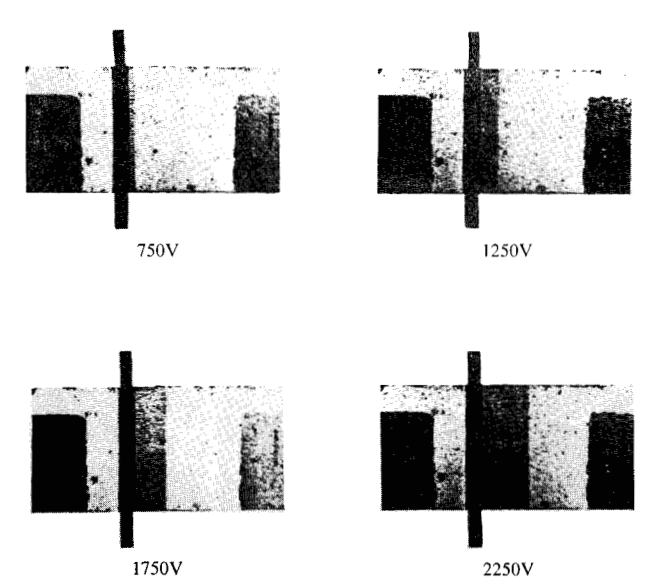
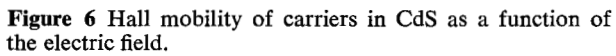
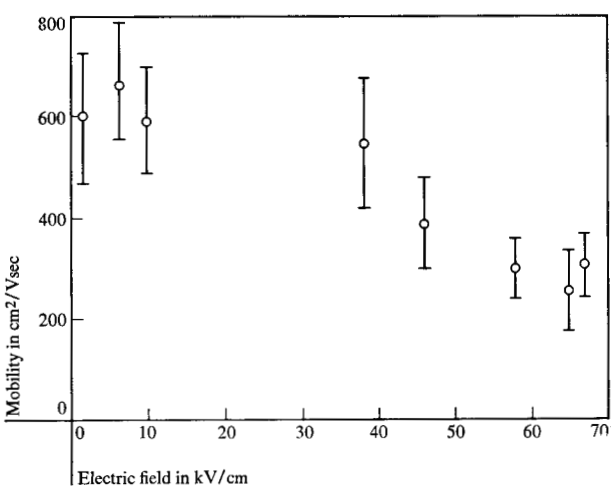


Figure 5 Photographs similar to those in Figure 2, illuminated as shown in Figure 4.





again unambiguously $\mu(E)$, as given in Fig. 6. It shows that μ decreases above 30 kV/cm approximately as E^{-1} , as expected for electron heating and optical phonon scattering.

With $\mu(E)$, finally n(E) can be calculated and is given in Fig. 7, which shows a behavior similar to the one assumed for the general discussion (Fig. 1).

Transition between stationary and moving domains

If the domain width surpasses a critical length, which is a function of crystal doping and cathode-boundary-condition, the current starts to oscillate and the domain becomes nonstationary.

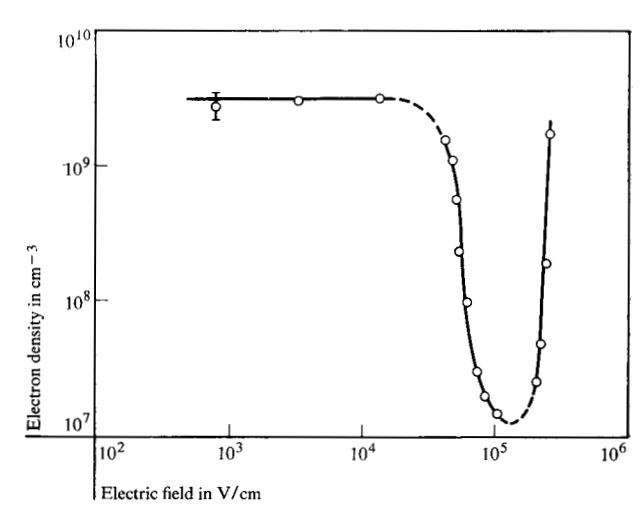
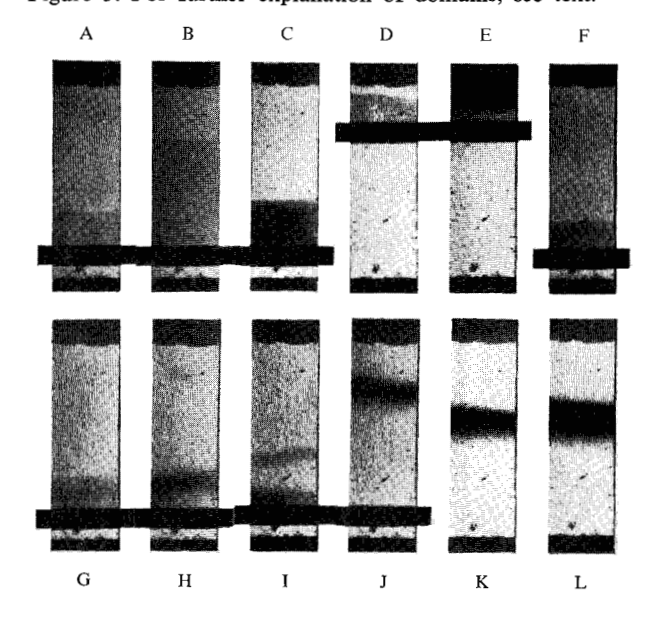


Figure 7 Electron density as a function of the electric field, calculated for zero space charge.

Figure 8 Photographs of CdS platelets similar to those in Figure 5. For further explanation of domains, see text.



At least two different types of nonstationary domains (moving from cathode towards anode) must be distinguished: Undeformed moving domains (Type III) and domains which move under major deformation (Type II). These types can most clearly be distinguished according to their shape as seen via Franz–Keldysh effect and in respect to their current-voltage characteristics. It is observed that the occurrence of one or the other type is clearly determined by the boundary condition and therefore the method of the pseudo-cathode is again applied.

Fig. 8 shows a series of photographs indicating different conditions for stationary (Type I, upper line) and non-

stationary domains (Type II and III, lower line). The photos A and B show that the domain width can increase from 2000 to 4000 V to a rather large magnitude (~2 mm) without instabilities occurring if the current density (or n_c) is kept high enough. With reduced n_c (darker shadow) the domain field increases and therefore the domain width decreases (photo C). Reducing the width of region R (compare Fig. 4) and for high current densities the domain can be pulled across the entire region R and an anode-adjacent domain can be observed without instabilities occurring (photos D and E), similarly to Figs. 2 and 3. However, for lower values of n_c , stationary domains can be observed only up to 1800 V (photo F). At 2000 V marked domain "fluctuations" occur (photo G) which become more pronounced at 2500 V (photo H). The domain starts to break up, the field becomes slightly larger at some part of the domain and decreases in the neighborhood. However, while moving, the domain starts to dissolve before it reaches the anode (photo I) and a new perturbation starts to form and to move. Only if the voltage is increased (or n_a lowered sufficiently) the domain amplitude can increase sufficiently and its shape becomes "locked"; it then moves undeformed (photo J). The width of such Type III domain increases proportionally to the applied voltage (photos K and L), indicating flat-top domains.

The current-voltage characteristics corresponding to Fig. 8 are given in Fig. 9. Curve j_{hom} is calculated for a homogeneous field throughout the entire crystal. Curves 1 to 9 are directly measured with successively lowered carrier density in region Q (pseudo-cathode). With high $n_c(Q)$ no oscillation occurs (1 and 2). Lowering n_c small oscillations occur (indicated by dashed envelope) which disappear again for higher voltages (3). A similar behavior seems to shine through in curve 4, however overridden by another effect, which finally causes the domains to flip into the Type III (arrows at 5 and 6).

In contrast to Type II, the Type III domains show a well defined J-V characteristic, J_{mov} , independent of n_c as long as they are not too close to one electrode.

It is remarkable that the oscillation frequency of Type II domains decreases markedly with decreasing n_o , and that the current oscillates nearly symmetrically about the saturation current. Finally, for saturation currents below j_{hom} only stationary domains are observed. The regions for existence of different domain types are best seen in Fig. 10, however, the relative size of these regions vary greatly with different doping.

Theories of transitions between stationary and nonstationary domains

Several important features of these transitions can be obtained from a highly simplified one-level model, using field enhanced recombination as a process for the negative

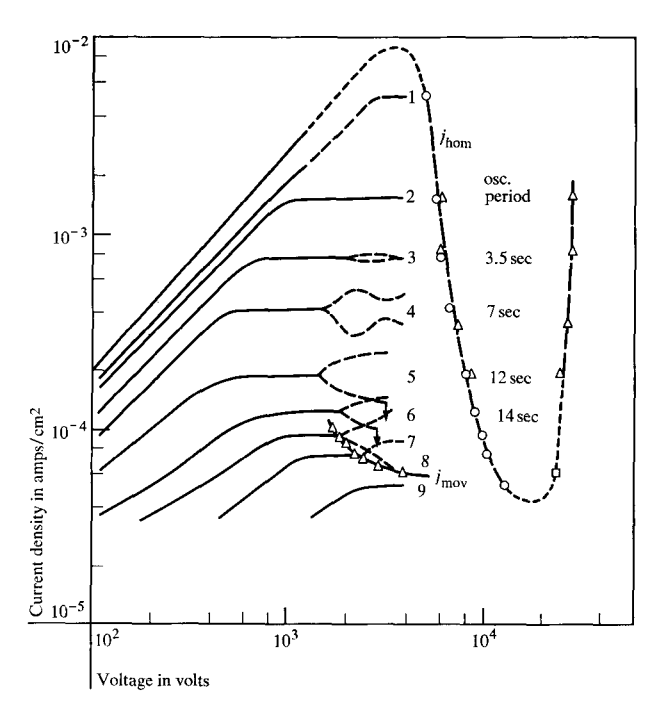


Figure 9 Current-voltage characteristics for successively reduced electron densities (from 1 to 9) at the pseudocathode (Q in Figure 4).

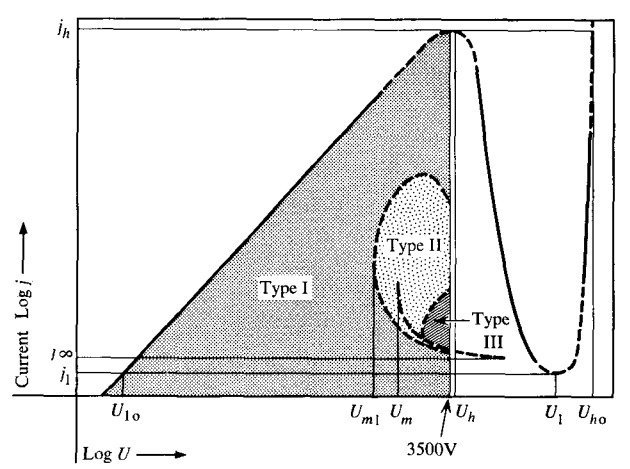


Figure 10 Generalized current-voltage characteristics to show ranges from Type I, II, and III domains.

differential conductivity, as long as linearization is a sufficient approximation, and the effective kinetic parameters are supplied from the experiment. This is justified for small amplitude Type II oscillations, and therefore should especially hold for discussion of the transition point from Type I to Type II domains.

Döhler¹⁹ has analyzed Poisson and transport equations for such kinetic models, yielding stationary solutions $E_s(x)$, $n_s(x)$ and j_s . With the Ansatz $E(x, t) = E_s(x) + \Delta E_s(x) \exp(i\omega t)$, $n_s(x, t) = n_s(x) + \Delta n_s(x) \exp(i\omega t)$ and

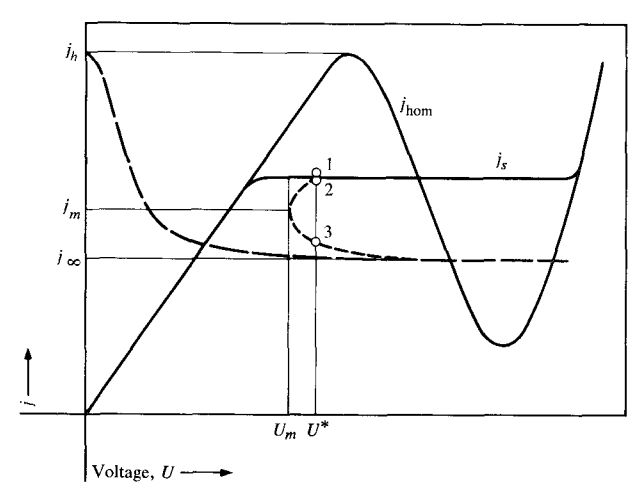


Figure 11 Current-voltage characteristics for stationary and moving domains. See text for description.

 $j_s(t) = j_s + \Delta j_s \exp(i\omega t)$ he obtains a solution for $\Delta E(x)$ with

$$\Delta V = \int_0^L \Delta E(x) \ dx = R(\omega, \ V) \ \Delta j. \tag{2}$$

The so-defined resistance R is complex and yields two conditions for the real and imaginary part of R to vanish, indicating that current oscillations may occur even though $\Delta V = 0$. From the two R-conditions one obtains a critical frequency ω_c the oscillatory frequency of j, and a critical applied voltage V_c (i.e. a critical domain width d_c).

These values ω_e and d_e depend on the boundary condition and shall for the first onset of Type II oscillation fulfill the equation:

$$\frac{d_c}{\omega_c} = \frac{\alpha_0 E_{\rm II}}{r} \tag{3}$$

with $E_{\rm II}$ the field in the stationary domain, r the slope of the negative differential conductivity and α_0 a material constant. A comparison with the experiment shows that within the experimental errors ($\pm 5\%$) Eq. (3) is indeed fulfilled.¹⁸

Moreover, since R=0 is not single valued in V, the theory predicts a series of critical points d_{c1} , d_{c2} ··· for which transitions between stable and unstable solutions should occur. The ratio of d_{ci}/d_{ck} is in first approximation a number, which, for $d_{c2}/d_{c1}=7/3$. The experimentally observed ratio (Fig. 9, curve 3) is 2.2 in good agreement with the theory.

However, when the oscillation amplitude becomes too large, the linearized theory is no longer useful. (Therefore cessation of oscillations has been observed only for curve 3 in Fig. 9, for which the oscillations remain small.)

Some further information can be obtained from a semiempirical discussion by $\operatorname{Kr\"oll}^{20}$: If one adds the voltage drop across an undeformed moving domain (dashed curve in Fig. 11) to the measured j-V curve for a stationary domain (heavy solid curve) one obtains a multi-valued (dash-dotted) curve for $V > V_m$, which is the j-V curve for the crystal with a Type III domain. It is clear that for $V < V_m$ and/or $j < j_{\infty}$ no Type III domains are possible. Because of minimum entropy production Type III domains are stable only for $j_{\infty} < j < j_m$, and j_m as well as j_{∞} do not depend on boundary conditions. It is most probable that the current during oscillations of Type II domains must decrease below j_m for a transition to Type III to occur. This seems to be in good agreement with the results given in Fig. 9.

In conclusion it is pointed out that the essential results obtained for trap-controlled slow moving domains, namely the existence of three domain types dependent on boundary conditions and applied voltage, should most probably hold true for other simple kinds of field instabilities, as, e.g., observed in Ge; Au²²⁻²⁴ and the Gunn effect.²⁵ The method of analysis, which has proven to be very helpful can easily be applied to other high-field domains as exemplified in Refs. 8, 11 and 12. Finally it is mentioned that stationary domains can be used as a powerful tool to determine carrier densities and mobilities unambiguously as a function of the field strength and to determine the metal-semiconductor work function for finite current densities.

Acknowledgments

This summarizing report is based on work which started in 1959 in Berlin together with H. J. Hänsch, U. Kümmel and W. E. Wilhelm, and was later continued at Delaware University with the help of K. Bogus, G. Döhler, G. A. Dussel, J. Green, P. Massicot, P. L. Quinn and P. Voss. It is a great pleasure for me to express here my gratitude to these teams of co-workers for their essential help.

References

- K. W. Böer, Phys. Rev. 139, A1949 (1965), J. Phys. Chem. Solids 22, 123 (1961).
- 2. K. W. Böer and G. A. Dussel, submitted for publication.
- R. H. Bube, Photoconductivity of Solids, John Wiley and Sons, New York 1960.
- 4. B. K. Ridley, Proc. Phys. Soc. 82, 954 (1963).
- K. W. Böer, H. J. Hänsch and U. Kümmel, Z. Phys. 155, 460 (1959).
- 6. K. W. Böer, Z. Phys. 155, (1959).
- 7. W. Shockley, Bell Sys. Tech. J. 33, 799 (1954).
- K. W. Böer and P. L. Quinn, Phys. Stat. Sol. 17, 307 (1966).
- 9. G. Döhler, Phys. Stat. Sol. 19, 555 (1967).
- K. W. Böer and W. E. Wilhelm, Phys. Stat. Sol. 3, 1704 (1964).
- K. W. Böer and G. A. Dussel, Phys. Rev. 154, 292 (1967).

- 12. K. W. Böer and G. Döhler, Phys. Rev., submitted for publication.
- 13. K. W. Böer and P. Voss, *Phys. Stat. Sol.* 28, 355 (1968).
- 14. K. W. Böer and P. Voss, Phys. Rev. 171, 899 (1968).
- K. W. Böer, G. A. Dussel and P. Voss, Phys. Rev. 179, 703 (1969).
- K. W. Böer, G. Döhler, G. A. Dussel, P. Voss, Phys. Rev. 169, 700 (1968).
- 17. K. W. Böer and K. Bogus, Phys. Rev. 176, 899 (1968).
- 18. K. W. Böer and P. Voss, *Phys. Stat. Sol.* **30**, 291 (1968).
- 19. G. Döhler, Phys. Stat. Sol. 30, 627 (1968).
- 20 K.-E. Kröll, Solid State Communications 6, 691 (1968).

- 21. H. Kies and F. Stöckmann, Phys. Stat. Sol. 4, 117 (1964).
- 22. S. G. Kalashnikov and V. L. Bonch-Bruevitch, *Phys. Stat. Sol.* 16, 197 (1966).
- M. S. Kagan, S. G. Kalashnikov and N. G. Zhdanova, *Phys. Stat. Sol.* 11, 415 (1965) and 24, 551 (1967).
- V. L. Bonch-Bruevitch, S. H. M. Kogan, Sov. Phys. Sol. St. 7, 15 (1965).
- 25. J. B. Gunn, Solid State Communications 1, 88 (1963).

Received April 14, 1969